

Published in final edited form as:

J Biol Chem. 2006 December 1; 281(48): 37091–37101.

Molecular Mechanism of Membrane Docking by the Vam7p PX Domain^{*,□}

Stephanie A. Lee[‡], James Kovacs[‡], Robert V. Stahelin^{§,¶}, Matthew L. Cheever^{||}, Michael Overduin^{**}, Thanuja Gangi Setty^{‡‡}, Christopher G. Burd^{‡‡}, Wonhwa Cho[§], and Tatiana G. Kutateladze[‡]

[‡]From the Department of Pharmacology, University of Colorado Health Sciences Center, Aurora, Colorado 80045

[§]Department of Chemistry, University of Illinois at Chicago, Chicago, Illinois 60607

[¶]Department of Biochemistry and Molecular Biology, Indiana University School of Medicine-South Bend and the Department of Chemistry and Biochemistry, the Walther Center for Cancer Research, University of Notre Dame, South Bend, Indiana 46617

Department of Pharmacology, University of North Carolina at Chapel Hill School of Medicine, Chapel Hill, North Carolina 27599

^{**}CR-UK Institute for Cancer Studies, University of Birmingham, Birmingham, B15 2T, United Kingdom

^{‡‡}Department of Cell and Developmental Biology, University of Pennsylvania School of Medicine, Philadelphia, Pennsylvania 19104

Abstract

The Vam7p t-SNARE is an essential component of the vacuole fusion machinery that mediates membrane trafficking and protein sorting in yeast. Vam7p is recruited to vacuoles by its N-terminal PX domain that specifically recognizes PtdIns(3)P in the bilayers, however the precise mechanism of membrane anchoring remains unclear. Here we describe a molecular basis for membrane targeting and penetration by the Vam7p PX domain based on structural and quantitative analysis of its interactions with lipids and micelles. Our results derived from *in vitro* binding measurements using NMR, monolayer surface tension experiments and mutagenesis reveal a multivalent membrane docking mechanism involving specific PtdIns(3)P recognition that is facilitated by electrostatic interactions and accompanying hydrophobic insertion. Both the hydrophobic and electrostatic components enhance the Vam7p PX domain association with PtdIns(3)P-containing membranes. The inserting Val⁷⁰, Leu⁷¹, and Trp⁷⁵ residues located next to the PtdIns(3)P binding pocket are surrounded by a basic patch, which is involved in nonspecific electrostatic contacts with acidic lipids, such as PtdSer. Substitution of the insertion residues significantly reduces the binding and penetrating power of the Vam7p PX domain and leads to cytoplasmic redistribution of the EGFP-tagged protein. The affinities of the PX domain for PtdIns(3)P and other lipids reveal a remarkable synergy within the multivalent complex that stably anchors Vam7p at the vacuolar membrane.

*This research was supported by Grants GM071424 and CA95144 from the National Institutes of Health (to T. G. K.) and GM68849 (to W. C.) and the American Cancer Society, RSG0513601 (to T. G. K.). The costs of publication of this article were defrayed in part by the payment of page charges. This article must therefore be hereby marked "advertisement" in accordance with 18 U.S.C. Section 1734 solely to indicate this fact.

□The on-line version of this article (available at <http://www.jbc.org>) contains supplemental Fig. S1.

To whom correspondence should be addressed: Dept. of Pharmacology, University of Colorado Health Sciences Center, 12801 East 17th Ave., Aurora, CO 80045-0511. Tel.: 303-724-3593; Fax: 303-724-3663; E-mail: Tatiana.Kutateladze@UCHSC.edu

Phosphoinositides (PIs),² phosphorylated derivatives of phosphatidylinositol (PtdIns), regulate diverse biological processes including growth, vesicular trafficking, cytoskeletal rearrangement, and survival of cells (reviewed in Ref. 1). The inositol headgroup of PIs is reversibly phosphorylated at three positions yielding seven isoforms, which cluster in distinct intracellular membranes. The apparent segregation of PIs is important for the fine-tuned regulation of protein and membrane traffic and also provides reliable and handy markers of organelles, such as the plasma membrane, trans-Golgi network, early endosomes, and multivesicular bodies. PIs were first recognized to function as precursors of secondary messengers in various signal transduction cascades and later as docking sites for modular effectors. A number of cytosolic protein effectors that are recruited to membranes and activated through interactions with PIs have recently been identified and structurally or biochemically characterized. The major PI binding modules include the ANTH (AP180 N-terminal homology), ENTH (epsin N-terminal homology), FERM (four-point one, ezrin, radixin, moesin), FYVE (Fab1, YOTB, Vac1, EEA1), PH (pleckstrin homology), and PX (Phox homology) domains (reviewed in Refs. 2-5,50).

The PX domain was first identified within a set of eukaryotic proteins in 1996 and named after the two phagocyte NADPH oxidase subunits, p40^{phox} and p47^{phox} (7). Since then, it has been

²The abbreviations used are:

PI	phosphoinositide
PtdIns(3)P	phosphatidylinositol 3-phosphate
PX	Phox homology
SNARE	soluble <i>N</i> -ethylmaleimide-sensitive fusion protein attachment receptor
HSQC	heteronuclear single quantum coherence
DHPC	diheptanoyl phosphocholine
CHAPS	3-[(3-cholamidopropyl)dimethylammonio]-1-propanesulfonate
POPC	1-palmitoyl-2-oleoyl- <i>sn</i> -glycero-3-phosphocholine
POPS	1-palmitoyl-2-oleoyl- <i>sn</i> -glycero-3-phosphoserine
PtdIns	phosphatidylinositol
PtdSer	phosphatidylserine
EGFP	enhanced green fluorescent protein
MIL	membrane interaction loop
GST	glutathione <i>S</i> -transferase
CHAPS	3-[(3-chol-amidopropyl)dimethylammonio]-1-propanesulfonic acid.

found in at least 69 human and 15 yeast signaling proteins, protein kinases, PtdIns kinases and phospholipases (SMART). These proteins are implicated in a variety of physiological events playing fundamental roles in endocytosis, protein sorting, membrane trafficking, transcription, signaling, cell growth, differentiation, and proliferation (5,7-9). The PX domain consists of ~130 residues that are folded in a highly conserved three-dimensional structure despite little sequence similarity between the family members. A proline-rich region (PXXP), involved in the interaction with SH3 domains, and a set of basic residues, shown to coordinate PIs, comprise the most conserved elements. Of all PIs, PtdIns(3)P appears to be a primary target of the PX domain-containing proteins as the majority of them are found associated with PtdIns(3)P-enriched endosomes and vacuoles (Vam7p, sorting nexins (SNXs), p40^{phox}, Grd19p), though interactions with PtdIns(3,4)P₂, PtdIns(3,5)P₂, PtdIns(4,5)P₂, and PtdIns(3,4,5)P₃ have also been reported for p47^{phox}, SNXs, PI3K C2γ, CISK, FISH, and PLD1 (7,10-18). This lack of binding specificity distinguishes the PX module from the FYVE domain, an exclusive effector of PtdIns(3)P, and links it to the less selective PH domain.

The atomic resolution crystal and solution structures of seven (CISK, Grd19p, p40^{phox}, p47^{phox}, SNX12, SNX22, and Vam7p) PX domains in the free and PtdIns(3)P- or PtdIns(3,4)P₂-bound states have been determined (Refs. 19-24, Protein Data Bank I.D. 2CSK, 2ETT, and 1KQ6)³. All show a similar fold consisting of three to four α -helices connected by a long exposed proline-rich loop and capped by a three-stranded β -sheet. The PtdIns(3)P molecule is positioned in a relatively narrow and deep groove formed by the α -helical bundle and makes numerous hydrogen bonds with the most conserved basic residues of the PX domain. In the case of p40^{phox} and p47^{phox} PX domains, the PI binding is supported by nonspecific electrostatic interactions and by insertion of hydrophobic residues of an exposed loop into the membrane (25). An analogous loop of the Vam7p PX domain is involved in the interaction with micelles as adjacent basic residues recognize PtdIns(3)P (12). The solution structure of the ligand-free Vam7p PX domain reveals a well formed PtdIns(3)P binding pocket implying that the lipid binding may induce local but not global conformational changes in the domain (22).

The Vam7p t-SNARE (soluble *N*-ethylmaleimide-sensitive fusion protein attachment receptor) is unique among PX domain-containing yeast proteins, most of which belongs to the SNX family. It is an essential component of membrane and protein trafficking in yeast, mediating homotypic vacuole fusion in cooperation with other SNAREs, NSF, SNAP, Rab GTPases, Sec1/Munc18, and additional elements of the membrane fusion machinery. While the majority of SNARE proteins associate with membranes through their transmembrane regions or via covalently attached lipids, Vam7p is targeted to vacuoles by its amino-terminal PX domain that specifically recognizes PtdIns(3)P (12). Consequently, both the intact PX domain and the presence of PtdIns(3)P are required for the subcellular localization of Vam7p (12). Despite the critical role in Vam7p function, the precise mechanism by which the PX domain targets PtdIns(3)P-enriched membranes remains unclear. Here we present the molecular basis of membrane docking and penetration by the PX domain of Vam7p based on structural and quantitative analysis of its interactions with lipids and micelles. Our results, derived from *in vitro* binding measurements using nuclear magnetic resonance (NMR) and monolayer surface tension combined with data from mutagenesis experiments and the *in vivo* localization of fluorescently tagged proteins, provide novel insights into the membrane recruitment mechanism of Vam7p. The affinities of the PX domain for PtdIns(3)P and other lipids reveal a remarkable synergy within the multivalent complex which is responsible for the vacuole anchoring of Vam7p.

³Protein Data Bank, unpublished data.

EXPERIMENTAL PROCEDURES

Subcloning, Expression, and Purification of Vam7p PX Domain

DNA fragments encoding residues 2-122 of the yeast Vam7p PX domain were amplified by PCR and cloned in pGEX-2T vector (Amersham Biosciences). The protein was expressed in the *Escherichia coli* BL21 (DE3) pLysS strain in minimal media supplemented with $^{15}\text{NH}_4\text{Cl}$ (Cambridge Isotope) and glycerol (5 ml/liter) or in LB media. Bacteria were harvested by centrifugation after induction with isopropyl-1-thio- β -D-galactopyranoside (0.5 mM) and lysed using sonication or a French press (18,000 psi, 4 °C). The unlabeled and ^{15}N uniformly labeled GST fusion protein was purified on a glutathione-Sepharose 4B column (Amersham Biosciences). The GST tag was cleaved with thrombin (Sigma). The PX domain was exchanged into 20 mM Tris or d₁₁-Tris, pH 6.8 in the presence of 100 or 200 mM KCl, 1 mM perdeuterated dithiothreitol, 50 μM 4-amidinophenyl methane sulfonyl fluoride, and 1 mM NaN_3 , in 7% $^2\text{H}_2\text{O}/\text{H}_2\text{O}$ or in $^2\text{H}_2\text{O}$ and concentrated using Millipore concentrators (Millipore). The protein identity and purity were determined by FPLC analysis, SDS-PAGE, and ^1H NMR.

PCR Mutagenesis of Vam7p PX

Site-directed mutagenesis of the Vam7p PX domain was performed using a QuikChange kit (Stratagene). The following mutants were generated: V70A, L71A, R73A, W75A, I90A, a double mutant V70AL71A and a triple mutant V70AL71AW75A. The sequences of all mutant constructs were confirmed by DNA sequencing.

NMR Spectroscopy and Lipid Titrations

NMR spectra were recorded at 25 °C on Varian INOVA 500 and 600 MHz spectrometers. The ^1H - ^{15}N heteronuclear single quantum coherence (HSQC) spectra of 0.2 mM uniformly ^{15}N -labeled PX domain were collected using 1024 t_1 increments of 2048 data points, 96 number of increments and spectral widths of 7500 and 1367 Hz in the ^1H and ^{15}N dimensions, respectively. Lipid binding was characterized by monitoring chemical shift changes in the ^1H - ^{15}N HSQC spectra of the PX domain as C_4 - or C_{16} -PtdIns(3)P (Echelon Biosciences Inc.) were added stepwise to 2 mM, diheptanoyl phosphocholine (DHPC) (Avanti) to 502 mM CHAPS (Sigma) to 167 mM, 1,2-dicaproyl-*sn*-glycero-3-[phospho-L-serine] (PtdSer) (Avanti) to 42 mM, dodecylphosphocholine (DPC) (Avanti) to 150 mM, cyclohexylbutylphosphocholine (Anatrace) to 250 mM, dihexanoyl phosphocholine (Avanti) to 150 mM, 1-myristoyl-2-hydroxy-*sn*-glycero-3-phosphocholine (Avanti) to 200 mM and 1-myristoyl-2-hydroxy-*sn*-glycero-3-phosphate (Avanti) to 50 mM. Significant changes in the resonances were judged to be greater than the average plus one standard deviation. The K_D values were calculated by a nonlinear least-squares analysis using the Xmgr program and Equation 1,

$$\Delta\delta = \Delta\delta_{\max} \left(\frac{([L] + [P] + K_D) - \left(([L] + [P] + K_D)^2 + (4 \times [P] \times [L])^{1/2} \right) / (2 \times [P])}{[L]} \right) \quad (\text{Eq. 1})$$

where [L] is the lipid concentration, [P] is the protein concentration, $\Delta\delta$ is the observed chemical shift change, and $\Delta\delta_{\max}$ is the chemical shift change at saturation. Micellar concentration, which corresponds to the solution concentration of intact micelles, was obtained by dividing the value of the detergent molecular concentration by an average aggregation number. Measured by pulse field gradient NMR (26), aggregation number for the mixed micelles comprised of DHPC and CHAPS (3:1 ratio) was found to be 40 molecules of DHPC and 13 molecules of CHAPS. The intensity profiles were standardized against those obtained for DPC micelles and cytochrome *c* under similar conditions (27).

Paramagnetic Spin Labels

The 5-, 10-, and 14-doxyl derivatives of 1-palmitoyl-2-stearoyl-sn-glycero-3-phosphocholine (3-6 mM) (Avanti) were gradually added to 250 μM ^{15}N -labeled PX domain in the presence of 1.25 mM $\text{C}_4\text{-PtdIns(3)P}$, 101 mM DHPC, and 35 mM CHAPS. The ^1H - ^{15}N HSQC spectra were collected after each addition of the spin lipids and intensities of backbone amide resonances were compared. The final ratio of spin label to micelle was between 0.7 and 1.3. The spin labels did not alter the structure of the protein based on the absence of chemical shift perturbations.

Monolayer Measurements

The penetration of wild-type and mutant Vam7p PX domains into the phospholipid monolayer was examined by measuring changes in the surface pressure (π) of invariable surface area while adding the protein. All experiments were performed at 23 °C using a 5-ml circular Teflon trough and Wilhelmy plate connected to a Cahn microbalance as previously described (28). A lipid monolayer containing various combinations of phospholipids was spread onto the subphase composed of 50 mM potassium phosphate, 0.16 M KCl, 1 mM dithiothreitol, and 1 mM NaN_3 at pH 7.0 until the desired initial surface pressure (π_0) was reached. After the signal stabilized, the PX domain was injected to a final concentration of 1 μM . The increase in surface pressure ($\Delta\pi$) was measured for 60 min while stirring the subphase at 60 rpm. Typically, the $\Delta\pi$ value reached a maximum after 25 min. The maximal $\Delta\pi$ value depended on the PX domain concentration and reached saturation at ~ 400 nM, therefore protein concentration in the subphase was maintained above this value. The resulting $\Delta\pi$ was plotted *versus* π_0 , and critical surface pressure (π_c) was determined as the x -intercept (29).

Liposome Binding

The liposome binding assays were performed as described in Ref. 30. Briefly, solutions of PC, PE, PtdSer (Avanti), PtdIns, and PtdIns(3)P (Echelon) dissolved in $\text{CHCl}_3\text{:MeOH:H}_2\text{O}$ (65:25:4) were mixed and dried down under vacuum. The lipids were resuspended in 50 mM Tris, 100 mM KCl, pH 7.0 and incubated at 64 °C for 1 h. The liposomes were then frozen in liquid nitrogen and thawed at 37 °C for three cycles. The liposome solution was passed through an Avanti extruder to make 1.0 μm liposomes. Liposomes were collected by centrifugation at $25,000 \times g$ for 10 min and resuspended to a final concentration of 2 mM total lipids in 100 μl 20 mM Tris, 100 mM KCl buffer, pH 7.4. Liposomes were incubated with the wild-type and mutant GST-Vam7p PX domain, GST or BSA (2 $\mu\text{g/ml}$ final protein concentration) for 30 min at room temperature and then collected again by centrifugation. The liposome pellets were resuspended in 100 μl of buffer and analyzed using SDS-PAGE with Coomassie Brilliant Blue staining.

The in Vivo Localization of Enhanced Green Fluorescent Protein (EGFP) Fusion Vam7p PX Domain in Yeast Cells

A region (amino acids 2-122) of Vam7p containing the wild-type or mutant PX domain was expressed in a wild-type yeast strain (BY4742) with an N-terminal EGFP tag using the pRS416-based expression vector, pGO-EGFP. Transformed strains were grown at 26 °C to an $A_{600} \sim 0.5$ in synthetic complete (SC) media lacking uracil to select for the plasmid. The cells were visualized by fluorescence microscopy as previously described (31). Images were acquired at the same exposure settings using Phase 3 Imaging software (Phase 3 Imaging Systems, Glen, PA) running on a Nikon Eclipse E800 microscope fitted with a cooled, high resolution charge-coupled device camera (model C4742-95, Hamamatsu Photogenics, Bridgewater, NJ). Site-directed mutagenesis was used to generate EGFP-PX domain mutants, I90A, V70A/L71A, and V70A/L71A/W75A using a QuikChange kit (Stratagene).

RESULTS

An Exposed Loop of the Vam7p PX Domain Is Involved in the Interaction with Lipid Micelles

To investigate the structural nature of the membrane association of the Vam7p PX domain, a number of soluble membrane mimetics were probed in NMR experiments. Of seven micelle systems screened, a mixture of DHPC and CHAPS in a ratio of 3 to 1 produced a lipid environment in which the Vam7p PX domain remained structured at all concentrations of micelles tested. The presence of CHAPS had a stabilizing effect on the PX domain tertiary structure preventing its unfolding. Moreover, this detergent appears to be capable of restoring a fully structured native state of the PX domain that is partially unfolded by DHPC alone. Upon titration of mixed DHPC/CHAPS micelles into uniformly ^{15}N -labeled Vam7p PX domain, pre-bound to $\text{C}_4\text{-PtdIns(3)P}$, substantial amide chemical shift changes in ^1H ^{15}N HSQC spectra were observed. The most pronounced perturbations of the ^1H and ^{15}N resonances were detected for the Glu⁶⁶, Lys⁶⁷, Val⁷⁰, Leu⁷¹, Arg⁷³, Arg⁷⁴, Trp⁷⁵, Gln⁷⁶, and Arg⁷⁷ residues of the loop connecting helices $\alpha 1$ and $\alpha 2$ of the PX domain (Fig. 1, *a-c*). Mapping the chemical shift changes onto the Vam7p PX domain surface revealed a flexible and a fully solvent exposed protrusion or membrane interaction loop (MIL) (12). The Val⁷⁰-Leu⁷¹ hydrophobic sequence, Trp⁷⁵ and the two adjacent charged regions, Arg⁷³-Arg⁷⁴ and Gln⁷⁶-Arg⁷⁷, exhibited the largest changes suggesting that both hydrophobic and electrostatic interactions might be involved. These perturbations paralleled chemical shift changes seen in the ligand-free PX domain as mixed DHPC/CHAPS micelles were titrated in (Fig. 1, *d-f*) and were similar in directions to small changes observed upon addition of dodecylphosphocholine (DPC) micelles (12). An almost identical pattern of resonance perturbations in the ligand-free and PtdIns(3)P-bound state of the PX domain suggests a similar mode of DHPC/CHAPS association involving the MIL. Yet, the micelle binding of the PtdIns(3)P-bound protein appears to be much stronger judging by significant line broadening of NMR resonances, indicative of an intermediate-to-fast exchange regime on the NMR time scale and hence a higher affinity interaction.

DHPC/CHAPS Micelles Enhance the Vam7p PX Domain Interaction with PtdIns(3)P

To determine the effect of micelle binding on the PtdIns(3)P interaction, resonances of DHPC/CHAPS-associated Vam7p PX domain were monitored while $\text{C}_4\text{-PtdIns(3)P}$ was titrated in. Addition of PtdIns(3)P induced large amide chemical shift changes in a number of charged, polar, and aromatic residues, the majority of which reside in the $\beta 1$ - and $\beta 2$ -strands, in the $\alpha 1$ - and $\alpha 2$ -helices and in the MIL (Fig. 2, *a-c*). Although the three-dimensional fold of the Vam7p-PX/PtdIns(3)P complex remains unknown, the solution structure of the ligand-free protein indicates that the PtdIns(3)P binding pocket is largely preformed in the domain (22). This implies that the chemical shift changes observed in NMR spectra occurred primarily because of direct interaction with PtdIns(3)P rather than caused by a conformational change in the PX domain. Indeed, the most affected residues, when labeled on the surface of the Vam7p PX domain, reveal a compact PtdIns(3)P binding site located at the stem of the MIL. Similar resonance perturbations were seen in the free Vam7p PX domain during titration of PtdIns(3)P (Fig. 2, *d-f* and Ref. 12), suggesting that PtdIns(3)P occupies the same binding pocket. However in the presence of DHPC/CHAPS micelles, resonances of the active site residues became significantly broader, indicating intermediate exchange and stronger binding. Thus, nonspecific association of the Vam7p PX domain with membrane-mimicking lipid systems enhances its specific interaction with PtdIns(3)P.

Affinities of the Vam7p PX Domain for Membrane Components

To quantitatively define the contribution of the nonspecific micelle association and PtdIns(3)P binding, dissociation constants (K_D) of each reaction were measured by NMR (Fig. 3). The magnitude of chemical shift changes in ^1H - ^{15}N HSQC spectra induced by PtdIns(3)P or DHPC/CHAPS micelles was evaluated for a number of substantially perturbed PX residues. As shown

in Fig. 3, PtdIns(3)P was bound by the free Vam7p PX domain with a K_D of $344 \pm 27 \mu\text{M}$, as determined from chemical shift perturbation analysis (Fig. 3a). However in the presence of DHPC/CHAPS micelles, the same interaction was seven times stronger, showing an affinity of $50 \pm 10 \mu\text{M}$ (Fig. 3b). Similar binding enhancement was exerted by PtdIns(3)P on the micelle association of the PX domain. That is, the DHPC/CHAPS micelle affinity of the ligand-free Vam7p PX domain was six times weaker ($7.1 \pm 1.6 \text{ mM}$) than that of the C_4 -PtdIns(3)P-bound PX domain ($1.2 \pm 0.2 \text{ mM}$, Fig. 3, c and d). The bivalent affinity of the Vam7p PX domain for C_4 -PtdIns(3)P-containing micelles, estimated as a product of the two sequential binding events (32), is then predicted to be $\sim 0.4 \mu\text{M}$. Interestingly, comparably increased binding affinities were reported for the FYVE domain interactions with PtdIns(3)P and DPC micelles (27). Similar to the FYVE domain, such amplification may be attributed to an insertion of hydrophobic residues of the PX domain in the micelle interior and/or may reflect the preference for the exposed acyl chains of PtdIns(3)P to become buried inside a micelle. Accordingly, extending the PtdIns(3)P acyl chains or increasing the MIL hydrophobicity is likely to enhance this interaction. Indeed, the micelle-associated PX domain bound more tightly to a long chain di-palmitoyl (C_{16})-PtdIns(3)P than to the short chain form, as evidenced by their slow and intermediate exchange on the NMR time scale (Fig. 2a and supplemental Fig. S1).

Vam7p PX Domain Penetrates Monolayers

A number of PI-recognizing modules, including FYVE and ENTH domains as well as PX domains of p40^{phox} and p47^{phox} have been shown to insert hydrophobic elements into bilayers (25,27,33,34). To test whether the Vam7p PX domain is capable of penetrating membranes, we analyzed its ability to alter surface tension of lipid monolayers of different compositions. The monolayers containing POPC/POPS and POPC/POPS/PtdIns(3)P were spread onto a surface area with initial surface pressure of π_0 , and after the injection of the protein, the change in surface pressure ($\Delta\pi$) was measured (Fig. 4, a-c). As shown in Fig. 4a, the Vam7p PX domain exhibited low penetrating power into a POPC/POPS monolayer with a π_c value ~ 24 dyne/cm, implying that in the absence of PtdIns(3)P it has low intrinsic membrane-penetrating capability. However, incorporation of PtdIns(3)P into the monolayer substantially elevated its penetration raising the π_c value to ~ 33 dyne/cm. These results suggest that Vam7p can penetrate membranes since the surface pressure of cell membranes is estimated to be ~ 31 dyne/cm (35) and PtdIns(3)P binding is required for the strong insertion. Likewise, PtdIns(3)P is necessary for the FYVE domain to sufficiently penetrate phospholipid monolayers or micelles (27,33). The specific nature of the PtdIns(3)P effect on the Vam7p PX domain insertion was confirmed by the lack of an increase in surface pressure when phosphatidylinositol-5-phosphate (PtdIns(5)P) was incorporated into the monolayers (Fig. 4a).

The MIL Residues Val⁷⁰, Leu⁷¹, and Trp⁷⁵ Insert into the Micelle Interior

To identify the MIL residues penetrating membranes, NMR experiments with spin label probes were carried out. The paramagnetic 5-, 10-, and 14-doxyl-phosphatidylcholine lipids carry a nitroxyl radical at positions 5, 10, and 14 of the stearyl side chain, respectively. They readily incorporate into micelles and broaden NMR resonances of nuclei located near the micelle surface, in the middle of the lipid acyl groups and in the center of micelles, respectively, as was thoroughly measured by NMR and EPR studies (36-38). Consequently, protein residues buried in the center of micelles, residues partially penetrating the hydrophobic core and residues located at the micelle surface are expected to experience selective line broadening upon addition of 14-, 10-, and 5-doxyl probes, respectively. When 5- or 10-doxyl probes were added to the ¹⁵N-labeled Vam7p PX domain, which was pre-bound to C_4 -PtdIns(3)P and DHPC/CHAPS micelles, a significant reduction of the Val⁷⁰, Leu⁷¹, and Trp⁷⁵ amide signal intensities was observed (Fig. 5). In contrast, addition of the 14-doxyl probe caused no line broadening of amide resonances (data not shown). Thus, the Val⁷⁰, Leu⁷¹, and Trp⁷⁵ residues of the Vam7p

PX domain partially penetrate the hydrophobic core of the micelles. The depth of the insertion by the PX domain appears to be smaller than that of the EEA1 FYVE domain, whose hydrophobic residues entirely insert into the micelle interior (27). Furthermore, selective broadening of MIL resonances was not seen upon titration of any spin label into the PtdIns(3)P-free state of the micelle-saturated PX domain (data not shown), supporting the idea of superficial or transient nature of the Vam7p PX domain nonspecific micelle association.

Mutations of the Hydrophobic MIL Residues Diminish the PX Domain Membrane Association

To investigate the role of hydrophobic insertion in membrane targeting of the Vam7p PX domain, the MIL residues Val⁷⁰, Leu⁷¹, and Trp⁷⁵ were substituted for Ala. The single mutants (V70A, L71A, and W75A), a double mutant V70A/L71A and a triple mutant V70A/L71A/W75A were generated along with I90A, in which a solvent exposed hydrophobic Ile residue, distal to the MIL, was mutated as a control. Well dispersed resonances in one- and two-dimensional NMR spectra of the mutant PX domains suggested that they maintained a stable structure (data not shown). Initially, the mutant proteins were tested by liposome binding assays (Fig. 4d). To better mimic vacuolar membranes, liposomes were prepared from phospholipids commonly found in vacuoles and endosomes including PC, PE, PtdSer, PtdIns, and increasing concentrations of PtdIns(3)P. While the wild-type Vam7p PX domain or I90A mutant were found associated with PtdIns(3)P in the liposome fraction, the V70A, L71A, W75A, and V70A/L71A mutant proteins were equally partitioned between soluble and liposome-bound fractions. The V70A/L71A/W75A mutant was unable to bind PtdIns(3)P and primarily retained in the supernatant demonstrating the importance of hydrophobic interactions involving the Val⁷⁰, Leu⁷¹, and Trp⁷⁵ residues. When these residues are replaced, the strong anchoring of the Vam7p PX domain to PtdIns(3)P-containing bilayers is disrupted.

The critical role of the hydrophobic residues was further substantiated by monolayer surface tension experiments (Fig. 4, b and c). Replacement of Val⁷⁰/Leu⁷¹ and Val⁷⁰/Leu⁷¹/Trp⁷⁵ with Ala greatly reduced the penetrating capability of the PX domain decreasing the π_c values to 27 and 26 dyne/cm (Fig. 4c). While individual mutations of Val⁷⁰ and Trp⁷⁵ residues slightly diminished the PtdIns(3)P dependent penetration, substitution of Leu⁷¹ caused a significant decrease in penetrating power of the PX domain suggesting that insertion of the long hydrophobic side chain of this residue is required for sufficient docking to membranes (Fig. 4b). As expected, in a control experiment, I90A mutant penetrated monolayers to the same extent as the wild-type PX domain (Fig. 4b).

Hydrophobic Insertion Is Necessary for the *in Vivo* Localization of the Vam7p PX Domain

It has been shown that Vam7p is recruited to vacuoles through binding of its N-terminal PX domain to PtdIns(3)P, enriched in vacuolar membranes (12). To investigate the significance of penetration for *in vivo* localization of the Vam7p PX domain, EGFP fusion wild-type protein and V70A/L71A, V70A/L71A/W75A, and I90A mutants were generated and their subcellular distribution in yeast cells was examined by fluorescent microscopy. In agreement with previous reports, the wild-type EGFP-Vam7p PX domain was primarily localized to vacuolar membranes (Fig. 6). Similar membrane association was observed for the I90A mutant, in which the MIL region remained intact. In contrast, the MIL-defective mutants, V70A/L71A or V70A/L71A/W75A were evenly distributed in the cytosol and did not localize to vacuole membranes. Thus, the hydrophobic insertion by the MIL residues is required both, for the *in vitro* association of Vam7p PX domain with PtdIns(3)P-containing monolayers, bilayers, and micelles and for anchoring of the protein to yeast vacuoles *in vivo*.

Nonspecific Electrostatic Interactions with PtdSer Enhance the PX Domain Binding to PtdIns(3)P-containing Micelles

The cytosolic leaflet of vacuolar and endosomal membranes is enriched in acidic phospholipids other than PtdIns(3)P including PtdSer, which is known to promote the membrane association of PI binding domains. To determine whether the nonspecific electrostatic contacts with acidic head groups contribute to the Vam7p PX domain recruitment to PtdIns(3)P-containing membrane mimetics, we examined its interaction with PtdSer. NMR titration of soluble dicaproyl (C₆)-PtdSer into the PX domain, which had been pre-bound to C₄-PtdIns(3)P and DHPC/CHAPS micelles, caused significant chemical shift changes in residues located in and around the MIL and PtdIns(3)P binding site (Fig. 7). These perturbations suggest that PtdSer binding involves charged and polar residues including Lys⁴⁰, Arg⁴¹, Lys⁴⁷, Lys⁷³, Gln⁷⁶, and Arg⁷⁷ that form a predominantly basic patch and may easily accommodate a PtdSer headgroup next to the bound PtdIns(3)P molecule.

The electrostatic contacts with PtdSer further the Vam7p PX domain interaction with PtdIns(3)P embedded in micelles. When DHPC/CHAPS micelles containing 10% C₆-PtdSer were gradually added to C₄-PtdIns(3)P-bound PX domain, the majority of the MIL resonances and resonances of several PtdIns(3)P-binding site residues disappeared in ¹H ¹⁵N HSQC spectra. Such rapid loss of signals indicates intermediate exchange on NMR time scale and stronger binding than that in the absence of PtdSer (Fig. 3, *d* and *e*).

To examine the contribution of the nonspecific electrostatic interactions in the Vam7p PX domain membrane association, Arg⁷³ residue was substituted for Ala and the corresponding mutant protein was probed by liposome binding and monolayer penetration assays. The Arg⁷³ residue was chosen among other perturbed basic residues because it does not coordinate the PtdIns(3)P head group nor is it involved in the insertion. Therefore, the effect caused by disrupting PtdIns(3)P binding or MIL penetration could be eliminated. As shown in Fig. 4*d*, the R73A mutant of the PX domain was bound to PtdIns(3)P-containing liposomes to a lesser degree than the wild-type protein. Furthermore, the R73A mutation diminished the PX domain penetration into POPC/POPS/PtdIns(3)P monolayers, particularly at a lower initial surface pressure (Fig. 4*b*). These data support the idea that nonspecific electrostatic contacts significantly aid to the Vam7p PX domain membrane docking. Taking into account that several basic residues besides Arg⁷³ may also be synergistically involved, a larger effect of the electrostatic interactions on membrane association of the Vam7p PX domain should be expected. As in the case of the p40^{phox} and p47^{phox} PX domains (25), a strong positive potential surrounding the MIL and PtdIns(3)P binding pocket of the Vam7p PX domain may facilitate the initial membrane association reinforcing PtdIns(3)P binding and alleviating the hydrophobic penetration.

DISCUSSION

In conclusion, our results reveal the multivalent molecular mechanism of membrane docking by the Vam7p PX domain involving stereospecific PtdIns(3)P recognition which is facilitated by stabilizing electrostatic interactions with other acidic lipids and is accompanied by the insertion of hydrophobic MIL residues into the membrane (Fig. 8). The soluble PtdIns(3)P molecule occupies a relatively deep pocket near the stem of the MIL and the inositol head group binding site remains unchanged when the lipid is embedded in DHPC/CHAPS micelles. Three hydrophobic residues located at the tip of the MIL, Val⁷⁰, Leu⁷¹, and Trp⁷⁵ are ideally positioned to penetrate membranes. The direct contact of these residues with lipid bilayers could be initially predicted from the structure of the ligand-free Vam7p PX domain (22). In the absence of a global conformational change, ligation of PtdIns(3)P in the binding groove would most certainly pull a part of the domain inside the membrane bilayer. In agreement,

chemical shift perturbation analysis, monolayer surface tension, liposome binding, and spin label experiments demonstrate that the Vam7p PX domain penetrates membrane mimetics including micelles, monolayers and liposomes. Particularly, Val⁷⁰, Leu⁷¹, and Trp⁷⁵ residues of the MIL insert into DHPC/CHAPS/PtdIns(3)P micelles and POPC/POPS/PtdIns(3)P monolayers with a physiological surface pressure value. Judging by substantial quenching of signal intensities in ¹H-¹⁵N HSQC spectra of the PX domain caused by a 10-doxyl paramagnetic probe, all three residues insert into the micelle interior, and among them, Leu⁷¹ plays a major role in membrane anchoring as determined by mutagenesis. When Leu⁷¹ is replaced with a smaller but still hydrophobic Ala residue, the penetrating power of the corresponding mutant protein is considerably reduced (from 33 to 28 dyne/cm). This indicates that the long hydrophobic side chain of Leu⁷¹ is deeply inserted and the small size of the Ala methyl group is not sufficient for the strong membrane anchoring. The Ala substitution of Val⁷⁰ and Trp⁷⁵ residues results in a similar but much smaller effect, while the double and triple mutants (V70A/L71A and V70A/L71A/W75A) largely lose their ability to penetrate PtdIns(3)P-containing monolayers or bind PtdIns(3)P-containing liposomes. Furthermore, the V70A/L71A and V70A/L71A/W75A mutations disrupt the EFGP-Vam7p PX domain *in vivo* localization to vacuolar membranes revealing that the hydrophobic penetration is essential for membrane targeting.

Alignment of the PX domain sequences shows conservation of the hydrophobic residues suggesting that the MIL insertion may represent a common feature of the PX domain family. Thus, the Bem1, CISK, CPK, FISH, Grd19p, p40^{phox}, p47^{phox}, and SNX3 contain hydrophobic and aromatic VPYV, IFG, MVLG, VYVGV, ILF, ILL, WFDG, and LPF sequences, respectively, in place of the Val⁷⁰, Leu⁷¹, and Trp⁷⁵ residues of Vam7p and the MIL occupies analogous conformations in all PX domain structures (19-24). Mutations of MIL residues, such as Trp⁸⁰ of p47^{phox} or Tyr⁹⁴ and Val⁹⁵ of p40^{phox}, decrease binding affinities of the p47^{phox} and p40^{phox} PX domains by 6-50-fold and abolish *in vivo* localization of these proteins (20, 25). Replacement of I171 in a less hydrophobic MIL sequence of PLD1 PX domain (ENMI) reduces binding of this protein to PtdIns(3,4,5)P₃-containing liposomes by a factor of 4 (39). Clearly, the MIL insertion comprises a critical component of membrane association of the PX domains.

Our data demonstrate that PtdIns(3)P is required for the robust insertion of the Vam7p PX domain since a weak association with DHPC/CHAPS micelles or POPC/POPS monolayers alone is not sufficient for the penetration. On the other hand, hydrophobic insertion enhances PtdIns(3)P binding and yields a ~0.4 μM affinity for the lipid imbedded in DHPC/CHAPS micelles in contrast to a 344 μM affinity for soluble C₄-PtdIns(3)P. Several other PX domains, particularly those of high specificity, are recruited to PI-containing vesicles with a comparable strength. The PX domains of Grd19p and Mdm1p bind PtdIns(3)P with a *K_D* of ~2 μM, while a 1.3 nM affinity was measured for the p40^{phox} PX domain interaction (5,25). The p47^{phox} PX domain displays a ~1.5 nM affinity toward PtdIns(3,4)P₂/PtdSer-enriched liposomes (25), while less selective PX domains in general bind much weaker. A number of PI binding modules including ENTH (34,40) and FYVE (33,41,42) domains penetrate interfacial and hydrocarbon layers of the membrane. Multivalent anchoring resulting from the specific recognition of a PI and insertion of a set of aliphatic and aromatic residues provides the strength and selectivity that are necessary for the proper functioning of these proteins. Like the Vam7p PX domain, other PI-recognizing modules bind membrane-embedded PIs several orders of magnitude more tightly than soluble lipids or isolated inositol headgroups (43-45). Mutations of the membrane-inserting residues of the FYVE (31,33) or ENTH (34,40) domains abolish or significantly decrease the membrane association leading to the disruption of the normal biological activities of these proteins. The wealth of reports accumulated to date suggests that the membrane penetration could be a fundamental principle by which lipid interacting modules are stabilized at membranes.

Membrane association of the PI-binding proteins is often facilitated by nonspecific electrostatic interactions. The Vam7p PX domain exhibits similar properties. The hydrophobic MIL residues and the PtdIns(3)P binding pocket of the Vam7p PX domain are surrounded by a number of basic residues that make electrostatic contacts with acidic lipids other than PtdIns(3)P. These contacts further amplify the binding affinity as the replacement of a single basic Arg⁷³ residue significantly diminishes the Vam7p PX domain membrane binding and penetration. Interestingly, a range of PX domain sequences contain charged residues adjacent to the hydrophobic MIL regions suggesting a common mode of interactions. The importance of nonspecific electrostatic interactions has been exemplified by the membrane docking of the p40^{phox} and p47^{phox} PX domains (25). Initial binding of these proteins to the negatively charged membrane surfaces is shown to alleviate specific recognition of a PI which in turn induces a hydrophobic insertion (20,25). In the case of the p47^{phox} PX domain, additional amplification is provided by binding of PtdSer or phosphatidic acid in a separate lipid binding site. Recently it has been shown that recruitment of the ENTH, ANTH, FYVE, and PH domains to PI-containing membranes is enhanced by nonspecific electrostatic interactions (34,46-48) revealing a common anchoring component in the membrane targeting mechanism of these structurally unrelated modules.

Overall, the data presented here establish a multivalent mechanism of the Vam7p PX domain recruitment to PtdIns(3)P-enriched membranes which involves a network of intermingled interactions such as specific PtdIns(3)P binding, hydrophobic insertion and nonspecific electrostatic interactions. This mode of multiple membrane contacts provides the overall affinity and lipid specificity necessary for accurate targeting of Vam7p to vacuolar membranes.

Acknowledgements

We thank R. Brunecky, S. Emr, and A. Sorkin for discussions.

REFERENCES

1. Roth MG. *Physiol Rev* 2004;84:699–730. [PubMed: 15269334]
2. Hurley JH. *Biochim Biophys Acta* 2006;1761:805–811. [PubMed: 16616874]
3. Kutateladze TG. *Biochim Biophys Acta* 2006;1761:868–877. [PubMed: 16644267]
4. Dinitto JP, Lambright DG. *Biochim Biophys Acta* 2006;1761:850–867. [PubMed: 16807090]
5. Seet LF, Hong W. *Biochim Biophys Acta* 2006;1761:878–896. [PubMed: 16782399]
6. Ponting CP, Onda T, Kitagawa M, Takeda O, Sago H, Kubonoya K, Inuma K, Bradley LA, Canick JA, Krasikov NE, Ponting NR, Grier RE. *Protein Sci* 1996;5:2353–2357. [PubMed: 8931154]
7. Zheng B, Ma YC, Ostrom RS, Lavoie C, Gill GN, Insel PA, Huang XY, Farquhar MG. *Science* 2001;294:1939–1942. [PubMed: 11729322]
8. Zhong Q, Lazar CS, Tronchere H, Sato T, Meerloo T, Yeo M, Songyang Z, Emr SD, Gill GN. *Proc Natl Acad Sci U S A* 2002;99:6767–6772. [PubMed: 11997453]
9. Lundmark R, Carlsson SR. *J Biol Chem* 2003;278:46772–46781. [PubMed: 12952949]
10. Kanai F, Liu H, Field SJ, Akbary H, Matsuo T, Brown GE, Cantley LC, Yaffe MB. *Nat Cell Biol* 2001;3:675–678. [PubMed: 11433300]
11. Ellson CD, Gobert-Gosse S, Anderson KE, Davidson K, Erdjument-Bromage H, Tempst P, Thuring JW, Cooper MA, Lim ZY, Holmes AB, Gaffney PR, Coadwell J, Chilvers ER, Hawkins PT, Stephens LR. *Nat Cell Biol* 2001;3:679–682. [PubMed: 11433301]
12. Cheever ML, Sato TK, de Beer T, Kutateladze TG, Emr SD, Overduin M. *Nat Cell Biol* 2001;3:613–618. [PubMed: 11433291]
13. Song X, Xu W, Zhang A, Huang G, Liang X, Virbasius JV, Czech MP, Zhou GW. *Biochemistry* 2001;40:8940–8944. [PubMed: 11467955]
14. Xu Y, Hortsman H, Seet L, Wong SH, Hong W. *Nat Cell Biol* 2001;3:658–666. [PubMed: 11433298]
15. Yu JW, Lemmon MA. *J Biol Chem* 2001;276:44179–44184. [PubMed: 11557775]

16. Xu J, Liu D, Gill G, Songyang Z. *J Cell Biol* 2001;154:699–705. [PubMed: 11514587]
17. Abram CL, Seals DF, Pass I, Salinsky D, Maurer L, Roth TM, Courtneidge SA. *J Biol Chem* 2003;278:16844–16851. [PubMed: 12615925]
18. Lee JS, Kim JH, Jang IH, Kim HS, Han JM, Kazlauskas A, Yagisawa H, Suh PG, Ryu SH. *J Cell Sci* 2005;118:4405–4413. [PubMed: 16179605]
19. Bravo J, Karathanassis D, Pacold CM, Ellson CD, Anderson KE, Butler PJ, Lavenir I, Perisic O, Hawkins PT, Stephens L, Williams RL. *Mol Cell* 2001;8:829–839. [PubMed: 11684018]
20. Karathanassis D, Stahelin RV, Bravo J, Perisic O, Pacold CM, Cho W, Williams RL. *EMBO J* 2002;21:5057–5068. [PubMed: 12356722]
21. Zhou CZ, de La Sierra-Gallay IL, Quevillon-Cheruel S, Collinet B, Minard P, Blondeau K, Henckes G, Aufrere R, Leulliot N, Graille M, Sorel I, Savarin P, de la Torre F, Poupon A, Janin J, van Tilbeurgh H. *J Biol Chem* 2003;278:50371–50376. [PubMed: 14514667]
22. Lu J, Garcia J, Dulubova I, Sudhof TC, Rizo J. *Biochemistry* 2002;41:5956–5962. [PubMed: 11993989]
23. Hiroaki H, Ago T, Ito T, Sumimoto H, Kohda D. *Nat Struct Biol* 2001;8:526–530. [PubMed: 11373621]
24. Xing Y, Liu D, Zhang R, Joachimiak A, Songyang Z, Xu W. *J Biol Chem* 2004;279:30662–30669. [PubMed: 15126499]
25. Stahelin RV, Burian A, Bruzik KS, Murray D, Cho W. *J Biol Chem* 2003;278:14469–14479. [PubMed: 12556460]
26. Altieri AS, Hinton DP, Byrd RA. *J Am Chem Soc* 1995;117:7566–7567.
27. Kutateladze TG, Capelluto DGS, Ferguson CG, Cheever ML, Kutateladze AG, Prestwich GD, Overduin M. *J Biol Chem* 2004;279:3050–3057. [PubMed: 14578346]
28. Bittova L, Sumandea M, Cho W. *J Biol Chem* 1999;274:9665–9672. [PubMed: 10092653]
29. Cho W, Bittova L, Stahelin RV. *Anal Biochem* 2001;296:153–161. [PubMed: 11554709]
30. Lee SA, Eyson R, Cheever ML, Geng J, Verkhusha VV, Burd C, Overduin M, Kutateladze TG. *Proc Natl Acad Sci U S A* 2005;102:13052–13057. [PubMed: 16141328]
31. Kutateladze TG, Ogburn KD, Watson WT, de Beer T, Emr SD, Burd CG, Overduin M. *Mol Cell* 1999;3:805–811. [PubMed: 10394369]
32. Tochtrop GP, Richter K, Tang C, Toner JJ, Covey DF, Cistola DP. *Proc Natl Acad Sci U S A* 2002;99:1847–1852. [PubMed: 11854486]
33. Stahelin RV, Long F, Diraviyam K, Bruzik KS, Murray D, Cho W. *J Biol Chem* 2002;277:26379–26388. [PubMed: 12006563]
34. Stahelin RV, Long F, Peter BJ, Murray D, De Camilli P, McMahon HT, Cho W. *J Biol Chem* 2003;278:28993–28999. [PubMed: 12740367]
35. Marsh D. *Biochim Biophys Acta* 1996;1286:183–223. [PubMed: 8982283]
36. Van Den Hooven HW, Spronk C, Van De Kamp M, Konings RNH, Hilbers CW, Van De Ven FJM. *Eur J Biochem* 1996;235:394–403. [PubMed: 8631359]
37. Jarvet J, Zdunek J, Damberg P, Graslund A. *Biochemistry* 1997;36:8153–8163. [PubMed: 9201964]
38. Papavoine CH, Konings RN, Hilbers CW, van de Ven FJ. *Biochemistry* 1994;33:12990–12997. [PubMed: 7947703]
39. Stahelin RV, Ananthanarayanan B, Blatner NR, Singh S, Bruzik KS, Murray D, Cho W. *J Biol Chem* 2004;279:54918–54926. [PubMed: 15475361]
40. Ford MG, Mills IG, Peter BJ, Vallis Y, Praefcke GJ, Evans PR, McMahon HT. *Nature* 2002;419:361–366. [PubMed: 12353027]
41. Kutateladze TG, Overduin M. *Science* 2001;291:1793–1796. [PubMed: 11230696]
42. Diraviyam K, Stahelin RV, Cho W, Murray D. *J Mol Biol* 2003;328:721–736. [PubMed: 12706728]
43. Gaullier JM, Ronning E, Gillooly DJ, Stenmark H. *J Biol Chem* 2000;275:24595–24600. [PubMed: 10807926]
44. Dumas JJ, Merithew E, Sudharshan E, Rajamani D, Hayes S, Lawe D, Corvera S, Lambright D. *Mol Cell* 2001;8:947–958. [PubMed: 11741531]

45. Sankaran VG, Klein DE, Sachdeva MM, Lemmon MA. *Biochemistry* 2001;40:8581–8587. [PubMed: 11456498]
46. Lemmon MA, Ferguson KM. *Biochem J* 2000;350:1–18. [PubMed: 10926821]
47. Lemmon MA, Ferguson KM, Abrams CS. *FEBS Lett* 2002;513:71–76. [PubMed: 11911883]
48. Singh SM, Murray D. *Protein Sci* 2003;12:1934–1953. [PubMed: 12930993]
49. Grzesiek S, Stahl SJ, Wingfield PT, Bax A. *Biochemistry*. 1996
50. Itoh T, De Camilli P. *Biochim Biophys Acta* 2006;1761:897–912. [PubMed: 16938488]

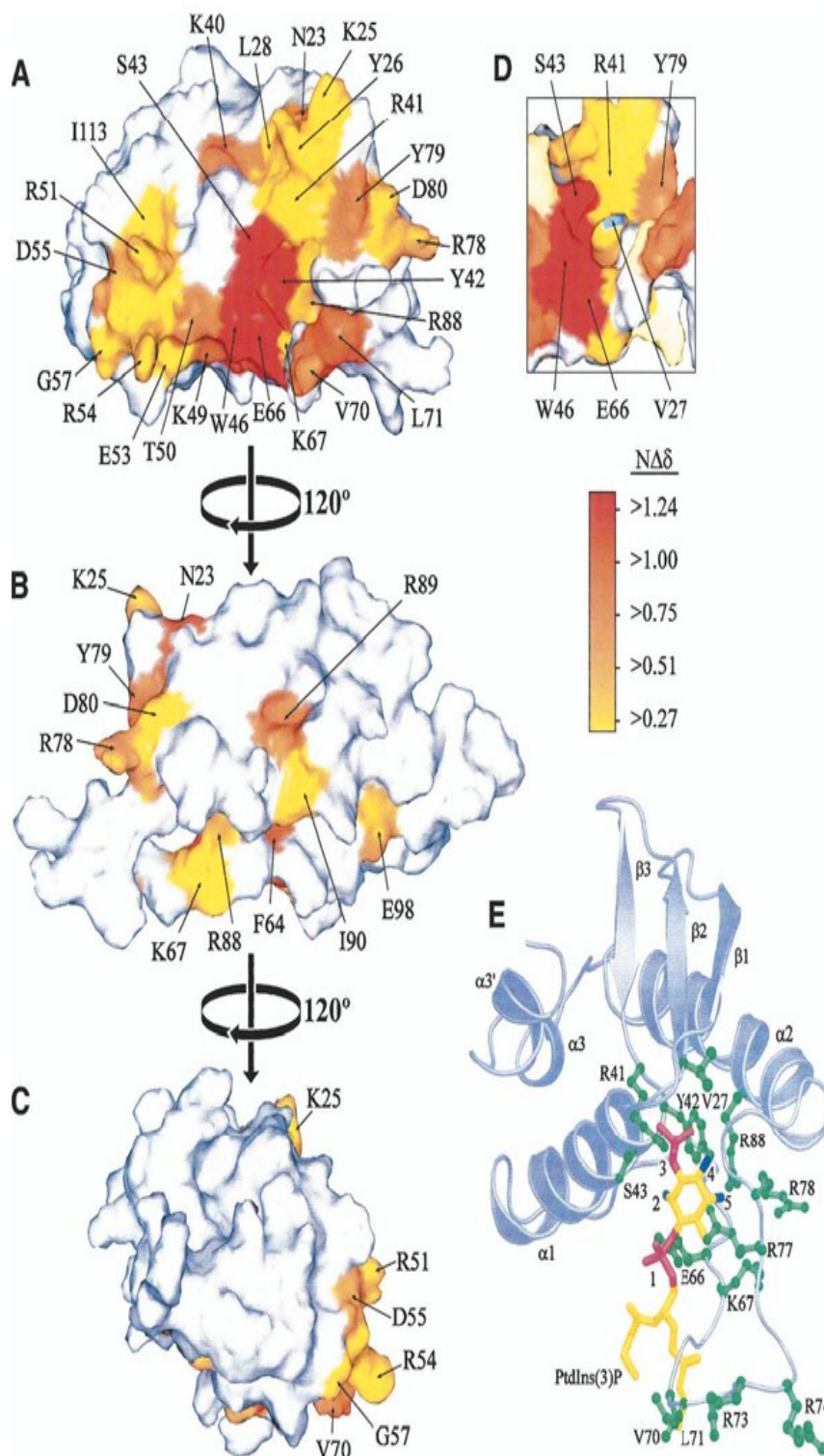


FIGURE 1. A long solvent-exposed loop of the Vam7p PX domain is involved in an interaction with micelles. Five superimposed ^1H - ^{15}N HSQC spectra of the PtdIns(3)P-bound (a) and the ligand-free (d)PX domain (0.2 mM) collected during titration with mixed DHPC and CHAPS (3:1

ratio) micelles are color-coded according to the indicated micellar concentrations of the lipids. The histograms show normalized (49) chemical shift changes induced in the backbone amide groups of the PtdIns(3)P-bound (*b*) and free (*e*) PX domain following addition of DHPC/CHAPS micelles. *c* and *f*, residues that exhibit significant DHPC/CHAPS micelle-induced resonance perturbations in *b* and *e* are labeled and colored in *red*, *orange*, *yellow*, and *gray* on the Vam7p PX domain (Protein Data Bank I.D. 1KMD) surface for large, medium, small, and insignificant changes, respectively.

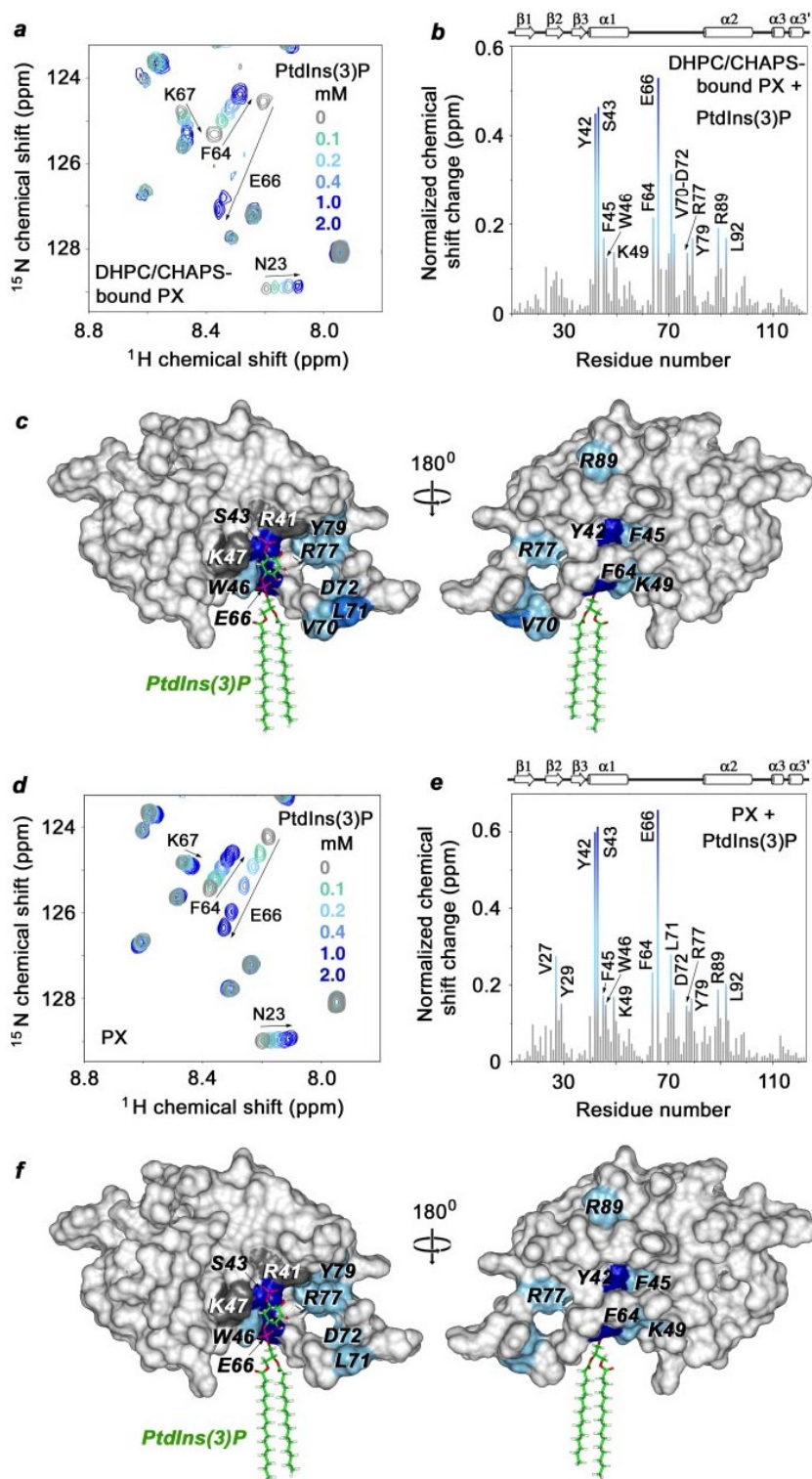


FIGURE 2. The DHPC/CHAPS micelle interaction enhances PtdIns(3)P binding of the Vam7p PX domain. Six superimposed ^1H - ^{15}N HSQC spectra of the micelle-bound (a) and unbound (d) PX domain (0.2 mM) collected as C_4 -PtdIns(3)P was gradually added. The NMR spectra are

color-coded as shown in the *insets* according to the concentration of PtdIns(3)P. The histograms display normalized chemical shift changes induced in backbone amides of the micelle-bound (*b*) and the micelle-free (*e*) PX domain upon titration of PtdIns(3)P. *c* and *f*, residues that exhibit significant resonance perturbations in *b* and *e* are labeled and colored in shades of *blue* on the PX domain surface.

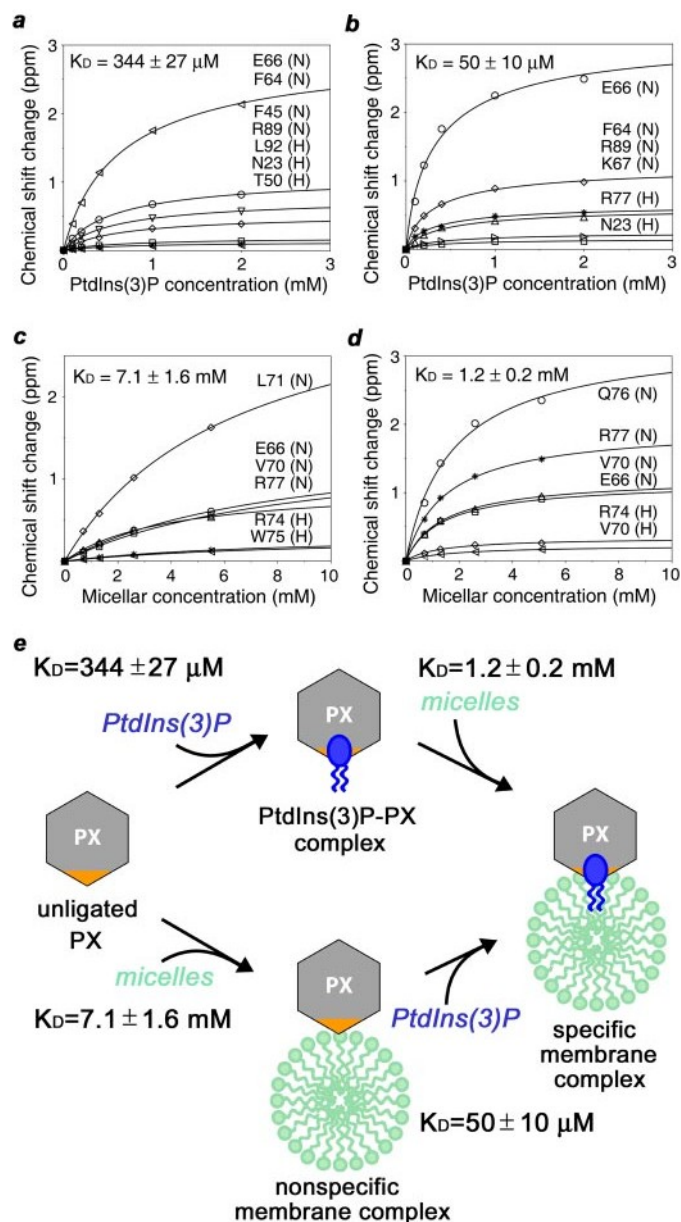
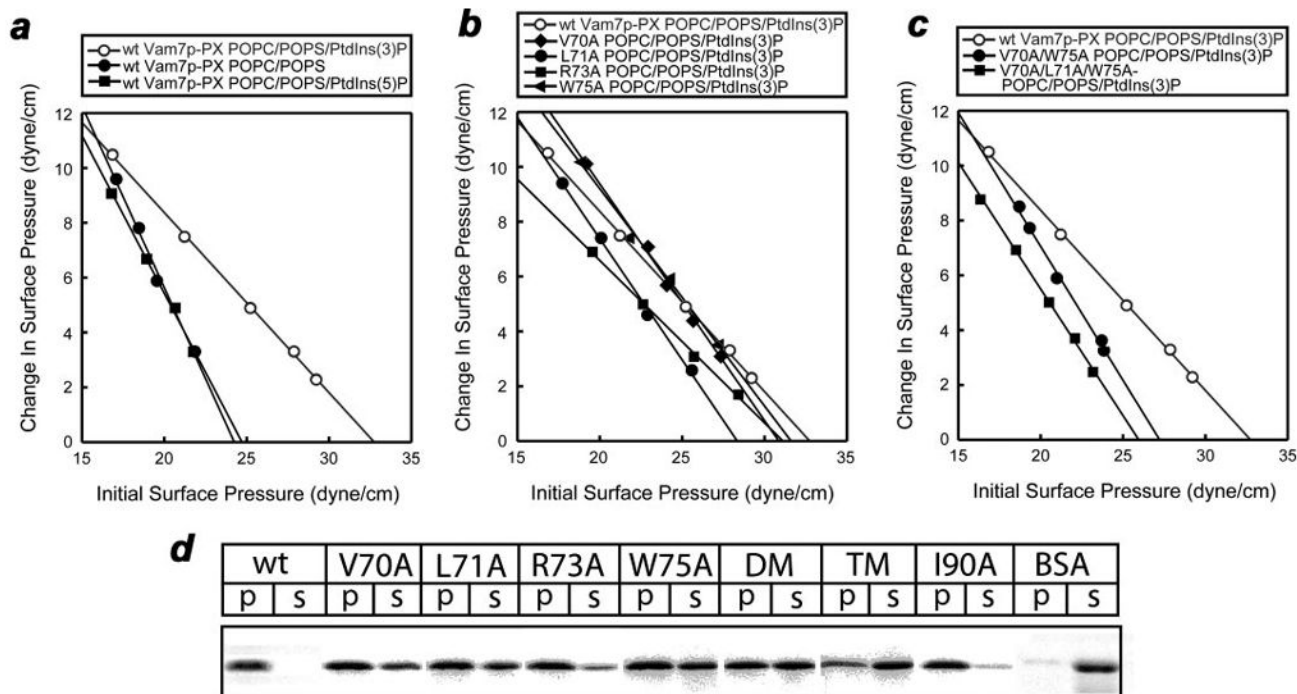


FIGURE 3. Affinities of the PX domain for C_4 -PtdIns(3)P and DHPC/CHAPS micelles. Titration of C_4 -PtdIns(3)P (*a* and *b*) and DHPC/CHAPS (*c* and *d*) into the PX domain induces changes in backbone ^{15}N and ^1H resonances, as observed in ^1H - ^{15}N HSQC spectra. The ^{15}N -labeled PX domain was initially either unbound (*a* and *c*), micelle-associated (*b*), or C_4 -PtdIns(3)P-bound (*d*). The estimated binding affinities are shown in the inset. *e*, model of sequential interactions of the PX domain with C_4 -PtdIns(3)P or DHPC/CHAPS micelles with monovalent affinities indicated.

**FIGURE 4.**

The effect of mutations in the MIL on the ability of the Vam7p PX domain to associate with PtdIns(3)P-containing liposomes and penetrate monolayers. *a*, graph showing changes in the surface pressure of POPC/POPS/PtdIns(3)P (82:15:3), POPC/POPS (85:15), and POPC/POPS/PtdIns(5)P (82:15:3) monolayers upon addition of the wild-type Vam7p PX domain. *b*, penetration of the wild-type and V70A, L71A, R73A, W75A and I90A Vam7p PX domain mutants into POPC/POPS/PtdIns(3)P (82:15:3) monolayers. *c*, penetration of the wild-type and V70A/W75A and V70A/L71A/W75A Vam7p PX domains into POPC/POPS/PtdIns(3)P (82:15:3) monolayers. *d*, the SDS-PAGE gels showing the partitioning of the wild-type and mutant Vam7p PX domain between the supernatant fraction (*S*) and PtdIns(3)P-enriched liposome pellet (*P*). The V70A/W75A and V70A/L71A/W75A Vam7p PX domain is denoted as the double (*DM*) and the triple (*TM*) mutant, respectively.

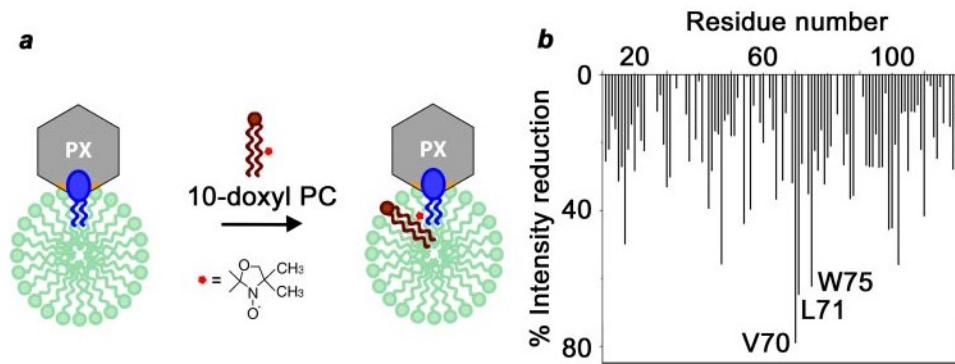


FIGURE 5. Insertion of the Val⁷⁰, Leu⁷¹, and Trp⁷⁵ MIL residues of the PtdIns(3)P-bound Vam7p PX domain into micelles. *a*, addition of a paramagnetic 10-doxyl probe (red) to the ¹⁵N-labeled Vam7p PX domain (gray hexagon) prebound to C₄-PtdIns(3)P (blue)-containing DHPC/CHAPS micelles (green) results in the loss of NMR signal intensities in hydrophobic residues of the MIL (orange). *b*, the histogram displays reduction of the resonance intensity in each residue backbone amide induced by 10-doxyl PC.

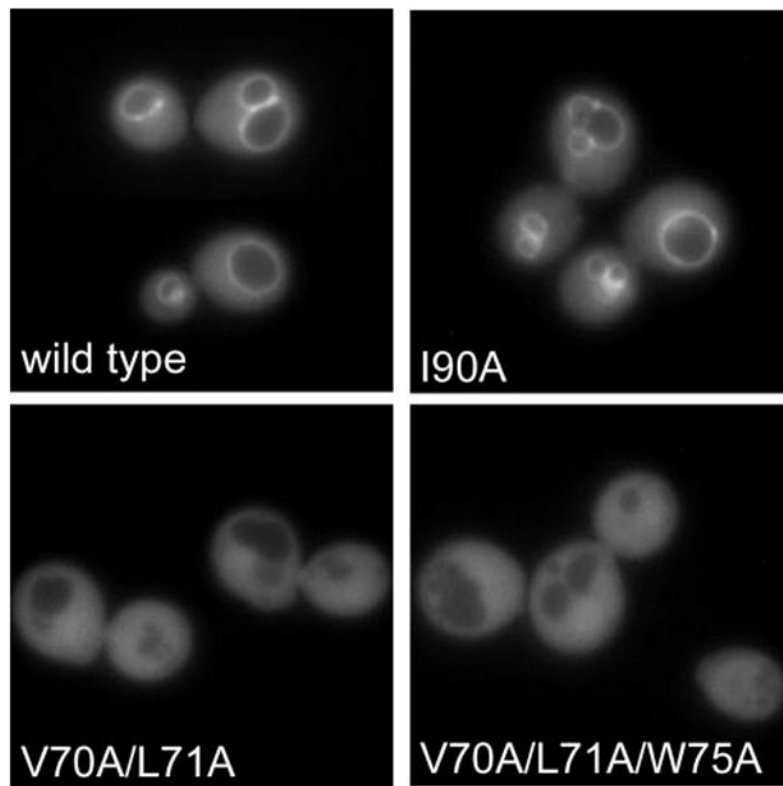


FIGURE 6. Substitution of the MIL residues disrupts the EGFP-Vam7p PX domain localization to vacuolar membranes in yeast cells. *In vivo* localization of the EGFP-fusion wild-type and V70A/L71A, V70A/L71A/W75A, and I90A mutant PX domains examined by fluorescence microscopy.

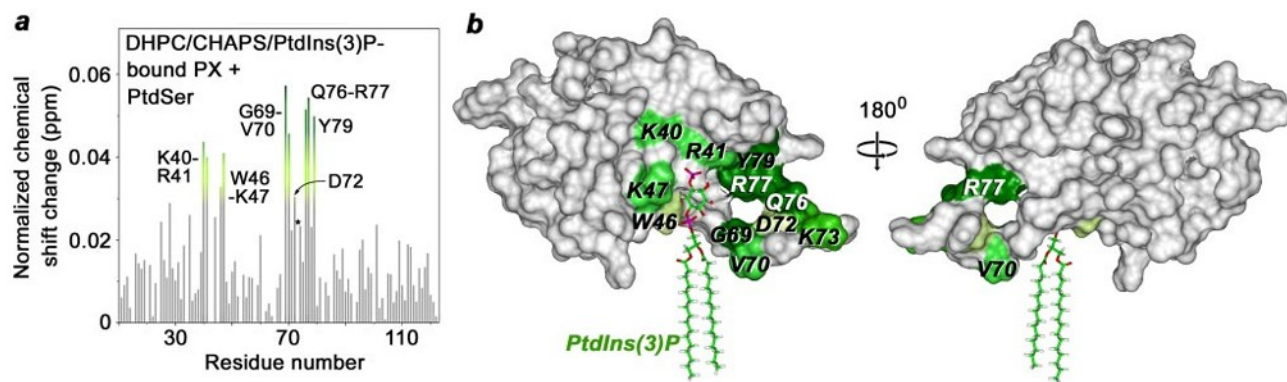


FIGURE 7. Interaction of the DHPC/CHAPS micelle- and PtdIns(3)P-bound Vam7p PX domain with PtdSer. *a*, the histogram shows normalized ^1H , ^{15}N chemical shift changes in backbone amides of the PX domain (0.2 mM) complexed with C_4 -PtdIns(3)P (2 mM) and DHPC/CHAPS (140 mM) upon titration of C_6 -PtdSer (up to 30% w/w). An *asterisk* points to the Arg⁷³ residue, whose amide resonance, initially showing a large change, disappears after addition of $\sim 10\%$ of PtdSer. *b*, residues that exhibit significant PtdSer-induced resonance perturbations in *a* are labeled and colored in shades of *green* on the PX domain surface.

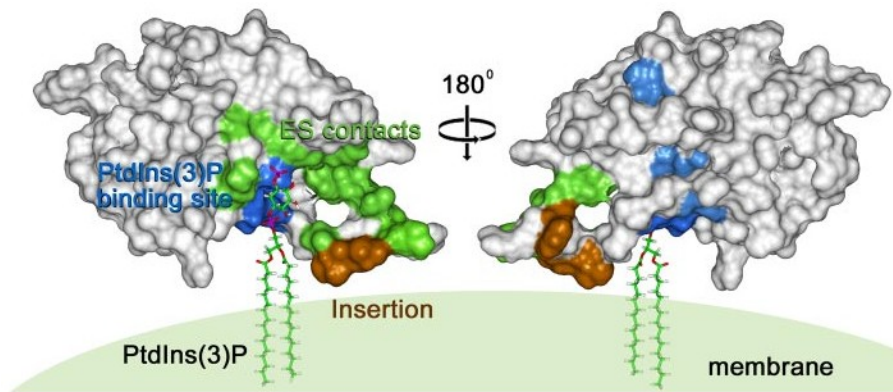


FIGURE 8.
A model of the Vam7p PX domain docking to PtdIns(3)P-containing membranes.
 Orthogonal views of the PtdIns(3)P-bound PX domain are shown with PtdIns(3)P binding site, the MIL insertion residues and PtdSer-interacting residues colored *blue*, *orange*, and *green*, respectively. The multivalent mechanism of the PX domain recruitment to vacuolar membranes involves stereospecific PtdIns(3)P recognition, which is facilitated by nonspecific electrostatic (*ES*) contacts with other acidic lipids and is accompanied by hydrophobic insertion.